

Prediction of Focal Image for Solar Parabolic Dish Concentrator With Square Facets – An Analytical Model

Arjun Singh Kopalakrishnaswami

NIT Puducherry: National Institute of Technology Puducherry

Reyhaneh Loni

Tarbiat Modares University

Ghoalmhosein Najafi

Tarbiat Modares University

SENDHIL KUMAR NATARAJAN (✉ drsendhil1980iitmuk@gmail.com)

National Institute of Technology Puducherry <https://orcid.org/0000-0003-3257-4570>

Research Article

Keywords: Paraboloid dish concentrator, square facet, focal image, confocal parameter, fringe size

Posted Date: December 7th, 2021

DOI: <https://doi.org/10.21203/rs.3.rs-1067854/v1>

License:  This work is licensed under a Creative Commons Attribution 4.0 International License.

[Read Full License](#)

1 **Prediction of Focal Image for Solar Parabolic Dish Concentrator with Square Facets – An Analytical**

2 **Model**

3 **Arjun Singh Kopalakrishnaswami^a, Reyhaneh Loni^b, Gholamhassan Najafi^b, Sendhil Kumar Natarajan^{a*}**

4 ^a Department of Mechanical Engineering, National Institute of Technology Puducherry, U.T. of Puducherry, India

5 ^b Department of Mechanic of Biosystems Engineering, Tarbiat Modares University, Tehran, Iran.

6 ***Corresponding Author: sendhil80@nitpy.ac.in**

7

8 Abstract

9 Solar parabolic dish concentrator is one of the high-temperature applications of more than 400 °C for thermal and
10 electrical power generation. In the solar parabolic dish concentrator, the arrangement of reflectors over the surface
11 area is the significant factor for effective concentration of solar radiation. Also, focal image is one of the most
12 influencing parameters in the design of receiver. Among the various reflectors, the square shaped reflectors
13 (facets) are comparatively effective in converging the incoming radiations to attain better focal image. In this
14 regard, an attempt has been made to predict the focal image diameter of a solar parabolic dish concentrator with
15 a square facet of different influencing parameters using a novel mathematical model. The influencing parameters
16 considered for the study are aperture diameter, rim angle, and facet length of the dish concentrator. Based on the
17 proposed model, the focal image dimension and aperture area of a solar parabolic dish concentrator with square
18 facets can be predicted accurately for efficient design of a solar parabolic dish collector system. Finally, the
19 proposed model is validated with the experimentally obtained focal image diameter and it is observed that the
20 predicted result is in good agreement with the experimental one. Thus, the proposed model can be effectively
21 used for the design of parabolic dish system for sustainable development.

22 **Keywords:** Paraboloid dish concentrator; square facet; focal image; confocal parameter; fringe size.

23 Nomenclature

24	d	diameter of the solar image
25	f	focal length of the parabolic dish
26	D	rim diameter of the parabolic dish
27	L	length of a facet
28	y	depth of parabola
29	x'	horizontal width of dish exposed to solar radiation
30	f ₁ , f ₂	Intersection point of extreme reflected rays at the axis of the parabola
31	f*	Actual solar image location from the apex
32		

33 Greek symbols

34	ω_0	half conical angle (0.266°)
35	ϕ	rim angle of the parabolic dish
36	α	horizontal inclination of facet at the extreme
37	ρ_1	horizontal inclination of reflected ray at point (x ₁ , y ₁)
38	ρ_2	horizontal inclination of reflected ray at point (x ₂ , y ₂)

39 1 Introduction

40 Energy is introduced as an essential measure for the all-around development of the nation although green
41 energy systems are considered essential for the sustainable development of the nation and the world. As the world
42 is encountering a huge rise in the populace, conventional energy resources are nearly getting drained. In this
43 situation, the world is moving towards non-conventional energy resources like solar energy, wind energy,

44 geothermal energy, salinity gradient power, and so on (Østergaard et al. 2020). The non-conventional energy
45 resources, solar energy is the most dominating and remarkable source of energy. The sun is a classic source of
46 energy that can satisfy the power needs of the whole earth. In contrast to other fossil fuels, the sun is a limitless
47 source of energy which is a critical hotspot in the future for clean energy. The fundamental limitations of using
48 solar power are more investment costs and accessibility of less efficient power transformation technologies.

49 Even though there exists a great deal of solar power transformation innovations accessible, the
50 concentrating solar power (CSP) technology draws in numerous researchers because of the capacity of producing
51 heat at a higher temperature. The concentrated solar parabolic dish (CSPD) collector system is one of the CSP
52 developments which concentrates the solar radiation to the most significant among the accessible inventions and
53 is generally competent among the available concentrated collectors (Kalogirou 2009). CSPD technology has
54 numerous applications where high temperature is required, for example, steam generation, pyrolysis process,
55 thermionic fluid heating for process heat applications, thermal energy storage systems, power generation using
56 Stirling engine, thermoelectric generators, concentrating photovoltaic, and so on. Aside, the capital expense of the
57 CSPD collector system is exceptionally high which is a significant barrier for commercialization (S P Sukhatme
58 and Nayak 2017). Hafez et al. have reviewed the design analysis factors of a solar parabolic dish for different
59 applications and performed a simulation of a solar parabolic dish with Stirling engine applications to determine
60 the efficiency and power outcome of the system (Hafez et al. 2016, 2017). Jian et al. proposed a novel optimization
61 method for the uniform distribution of solar flux in a cavity receiver of a solar parabolic dish concentrator system
62 (Yan et al. 2018). Premjit and Reddy investigated the flux distribution at the focal plane of a square solar parabolic
63 dish concentrator for concentrating photovoltaic application (Singh and Reddy 2020). Lan et al. performed an
64 optical simulation for determining the performance of a cylindrical cavity receiver for a solar parabolic dish
65 system (Xiao et al. 2020). Using a 4 m aperture diameter parabolic dish concentrator, Sahu et al. investigated a
66 flat receiver with a double trumpet shaped secondary reflector. In the parabolic dish, a square mirror facet was
67 used as a reflector element (Sahu et al. 2021).

68 Researchers have discovered fabrication of double-curved reflector panels are expensive and requests
69 advanced fabrication procedure, and subsequently thought of planar facets because of ease of fabrication (Toygar
70 et al. 2016). Although this process is affordable, the heat output is not sufficient because of the lack of established
71 relations to appraise the exact solar image. Lifang Li and Steven Dubowsky proposed another method for
72 fabricating the solar parabolic dish concentrators using flexible petals with optimum parameters. A numerical
73 study was led for the structure and an experimental study was performed with a prototype under the solar

74 simulator. Guaranteed that the proposed method will give exact solar parabolic dish collector and minimal cost
75 than the conventional method (Li and Dubowsky 2011). Researchers have attempted experiments to decide the
76 optimal solar image size and location. Pavlovic et al. led a ray-tracing simulation study to determine the optical
77 characteristics of the sun image size (Pavlovic´ et al. 2014). Sainath and Nitin performed a ray-tracing simulation
78 to study the possibilities of the reflector position and shape for a compound parabolic dish concentrator. Though
79 ray tracing simulation which is a numerical method available for the prediction of solar images the current paper
80 developed an analytical model for the determination of solar parabolic dish concentrator parameters (Waghmare
81 and Gulhane 2019). To estimate the distance between the concentrator and the receiver, Pavlovic et al. performed
82 optimization research on the parabolic dish concentrator with trapezoidal reflective pads (Pavlović et al. 2016).
83 Liu et al. proposed a new method by optimizing the size and placement of square facets in a solar parabolic dish
84 concentrator (Liu et al. 2012), Farouk et al. used the ray tracing technique to investigate the optical performance
85 of inverted absorber line axis compound parabolic concentrating solar collectors and published their findings in
86 terms of receiver height (Farouk Kothdiwala et al. 1996).

87 Wen et al. gave the geometrical optic relations to find the fringe diameter of a solar image for an ideal
88 parabolic dish concentrator (Wen et al. 1980). Afterward, Kaushika added an error to the conical angle which
89 occurred due to imperfections in optics and gave the solar image size for finding a multifaceted solar parabolic
90 dish concentrator (Kaushika 1993). This proposed analytical relation depended on the facet size and incident
91 angle. It is being utilized as the formula to decide the solar image size for the CSPD concentrator with facets.
92 Researchers used this relation to decide the fringe dimension for multiple applications (Hafez et al. 2017).
93 Nonetheless, the relation just connotes on the fringe dimension alone without mulling over its location. To find
94 the exact solar image location with more concentration ratio further computation needs to be done resulting in an
95 effective receiver for the respective parabolic dish concentrator. The computation is focused on deciding the solar
96 image with exactness and dependability for various facet lengths with varied parabolic profiles by geometrical
97 analysis through computer-aided simulations.

98 As seen from the aforementioned literature review, the focal image of the parabolic dish concentrator is
99 investigated as an important parameter for improving the total performance of the solar system. Consequently, the
100 main novelty of this study is to determine the actual solar image size and its location for a solar parabolic dish
101 concentrator with square facets as reflector elements using a new mathematical method. It should be mentioned
102 that graphical methods show that the existing relations leads to huge error and does not result in optimum solar

103 image location and dimension. The study takes into consideration the available facet size, conical angle of solar
104 rays as well as the other parameters of the dish.

105 **2 Modeling and Methods**

106 In the present work, an analytical model for finding the solar image dimension for a parabolic dish
107 concentrator using square facets was developed. Among the various reflectors, double curved facets are more
108 effective in converging the incoming radiations on the focal plane. However, the fabrication of double-curved
109 facets with high accuracy is complicated, expensive, and demands high skilled fabrication. As a better alternative,
110 square planar facets can be selected. Nevertheless, the features of square facets of appropriate dimensions are
111 almost similar to double planar facets with a minimum a deviation in flux distribution and focal image size.
112 However, these deviations can be compensated with the economic feasibility and ease of fabrication of square
113 facets. In this regard, the proposed method will provide a solution considering two cases: (i) the incoming solar
114 radiations as parallel rays. (ii) the conical angle possessed by the solar radiations. As a final part, studying the
115 shift in solar image position, the exact solar image location is concluded.

116 **2.1 General concepts**

117 The actual solar image border is defined by the radiations which are reflected by the rim elements of the
118 parabolic dish; hence the rim facet elements are considered for the derivation part. It is necessary to determine the
119 endpoints of the facets to determine the normal of the surface. The diameter and rim angle shown in Figure 1 gets
120 the extreme coordinates $((x_1, y_1) \& (-x_1, y_1))$ of the parabola. The rim facets have been created with the given
121 length (L) at the extreme coordinates of the parabola, where the second endpoint of facet $P_2 (x_2 \& y_2)$ can be
122 acquired from the relations below.

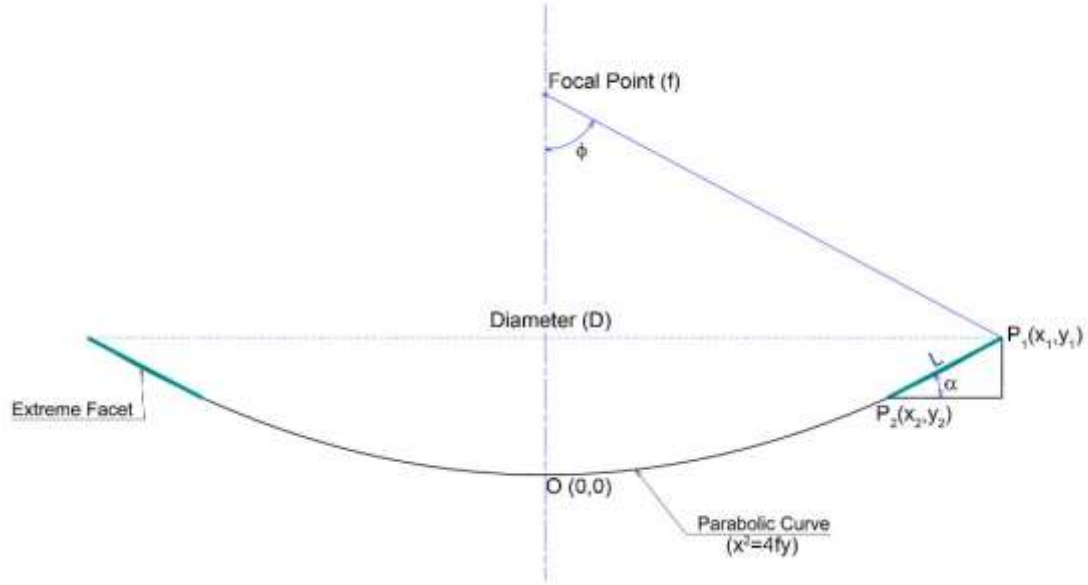


Figure 1: Parabolic dish with placement of facets at the extreme end

Equation of Parabola (Pavlovic and Stefanovic 2015) :

$$x^2 = 4fy \quad (\text{Explicit form}) \quad (1)$$

$$x = 2fu; \quad y = fu^2 \quad (\text{Parametric form}) \quad (2)$$

The extremities of a parabola can be found by the following expression

$$x_1 = \frac{d}{2} ; \quad y_1 = \frac{d^2}{16f} \quad (3)$$

Solving for the facet length using linear equation the following simplified quadratic equation

$$k^4 - 4u_1k^3 + 4u_1^2k^2 + 4k^2 - \frac{L^2}{f^2} = 0 ; \text{ where, } k = u_1 - u_2 \quad (4)$$

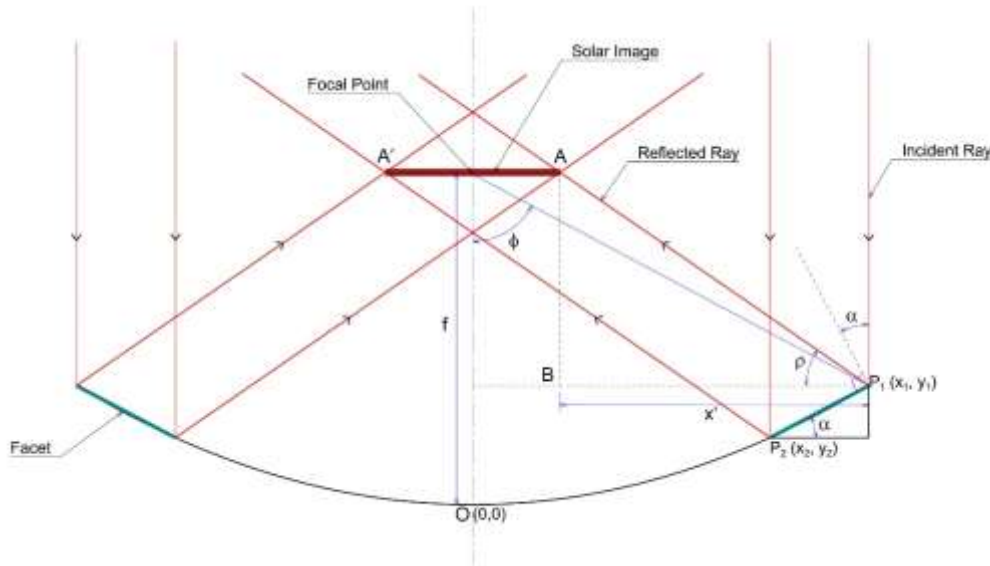
From the roots of the quadratic equation (eqn. 4), the coordinates of the facet end points can be determined.

2.2 Solar image diameter for parallel incident rays to the axis

In a parabolic dish, the solar image boundary is formed by the reflected rays at the extreme points and the same is observed in computer-aided graphical simulation. Thus, for deriving the fringe diameter of the solar image, the extreme facets and the reflections at the ends of the facet are taken. The intersection points of these reflections form the optimum solar image with maximum concentration ratio as demonstrated in Figure 2.

Two normal lines are created at points P₁ and P₂, endpoints of the extreme facet. The reflected rays for the incident vertical rays are obtained by Snell's law of reflection (angle of incidence with the normal is equal to

141 the angle of reflection with the normal) (Kingslake and Barry Johnson 2010) as shown in Figure 2. The line AA'
 142 joining the intersection of the extreme reflected rays gives the solar image.



143 **Figure 2: Solar Image formation of a parabolic dish concentrator with facets considering the solar rays as parallel.**

144 From Figure 2, based on trigonometric law, the expression for x' can be given as below.

$$145 \quad x' = \frac{f - y_1}{\tan(90 - 2\alpha)} \quad (5)$$

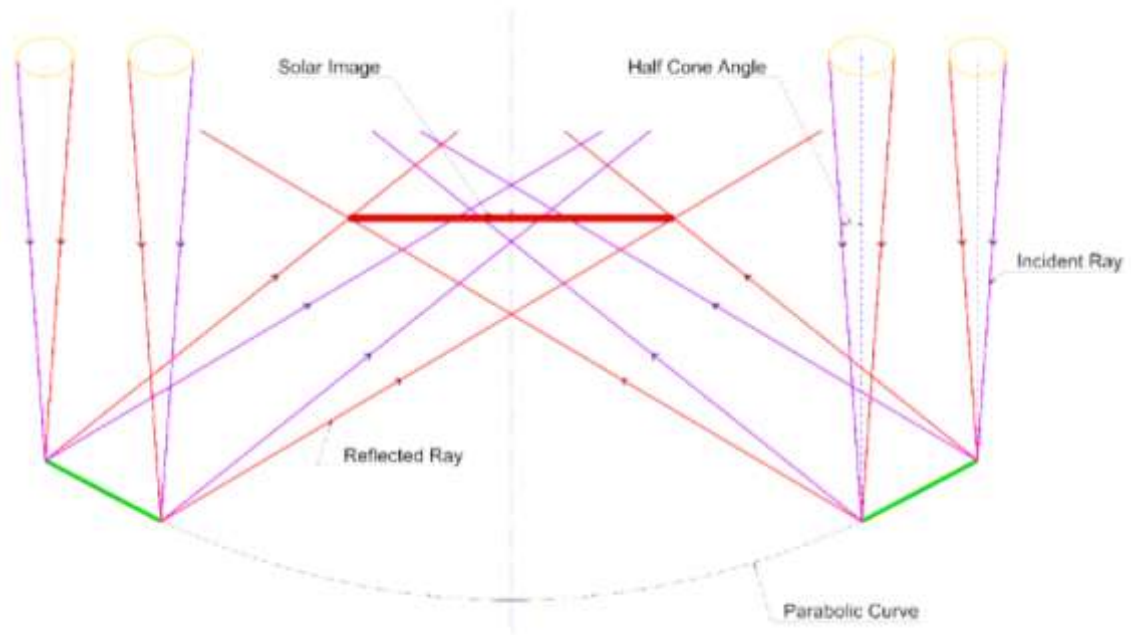
146 Hence, using the following expression (6), the solar image diameter of a solar parabolic dish concentrator
 147 with a square flat facet can be determined for the case, considering the solar rays as parallel.

$$148 \quad d = D - 2x' \quad (6)$$

149 The validation of the derived expression was conducted and from the obtained results, it was evident that
 150 the proposed model matches exactly with the geometrical simulation model.

151 **2.3 Solar image diameter considering the conical angle**

152 In the previous case, the radiations coming from the sun are assumed to be parallel. At the same time,
 153 there will be a maximum cone angle of 0.51° suspended by the incoming solar radiation (S P Sukhatme and Nayak
 154 2017). Though the conical angle is smaller, it acts upon the size of the concentrated solar fringe size. In Figure 3,
 155 the incident rays from the sun on the endpoints of the facets were shown. The incident rays are marked with red
 156 and violet colour. As the red-coloured incident rays reflect and make the boundary of the solar image, only those
 157 rays were considered in the determination of the solar image diameter.



159

Figure 3: Solar Image formation of a parabolic dish concentrator by considering the solar conical angle.

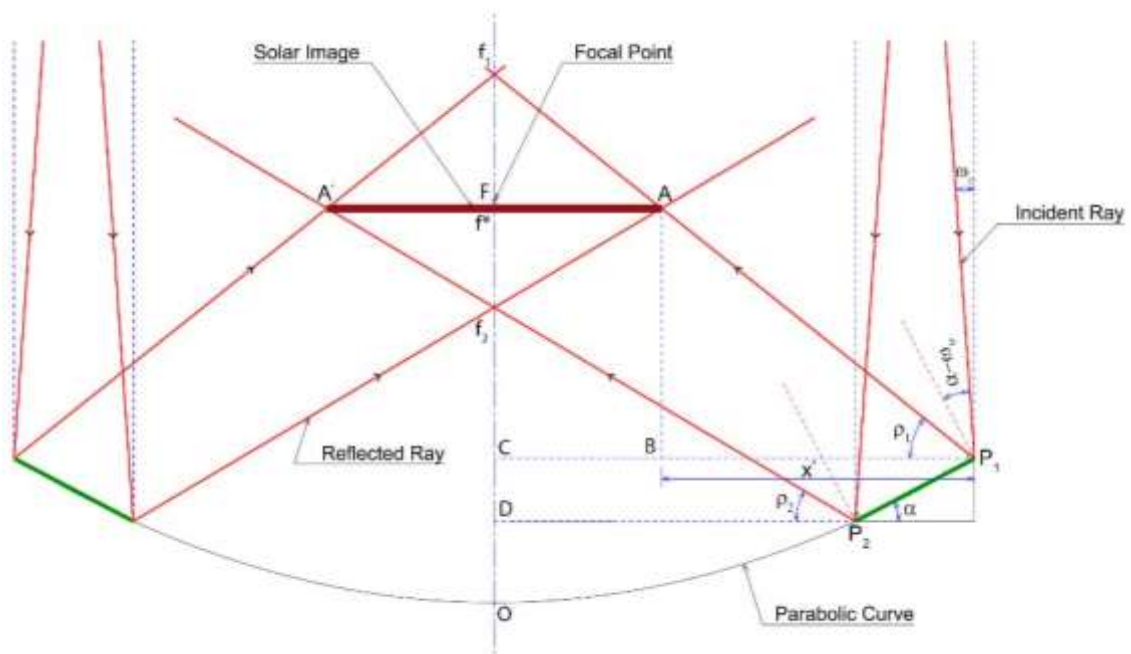
160

161

The construction of the parabolic dish with flat facets on the utmost ends of the parabola was done by considering the incident rays which generate the boundary of the solar image. The reflected geometry is produced and presented in Figure 4 as per Snell's law of reflection.

162

163



164

165

Figure 4: Solar Image based on extreme reflected rays.

166

From Figure 4, based on trigonometric law, the expression for x'' can be given as below.

167

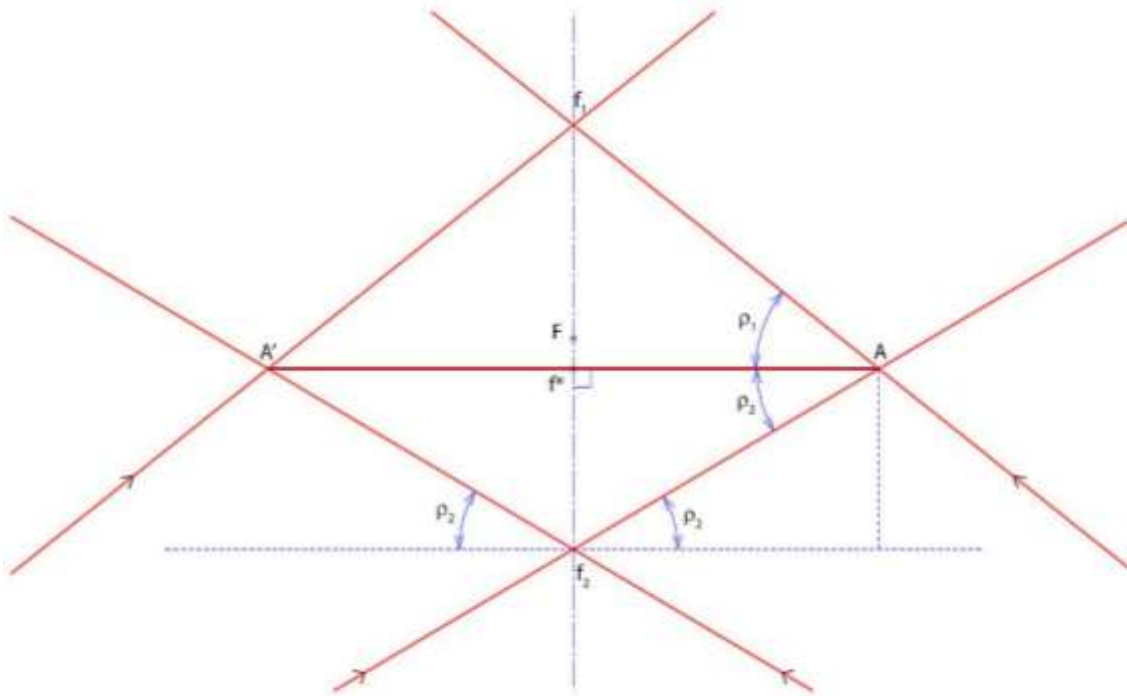
$$x'' = \frac{f^* - y_1}{\tan(90 - (2\alpha - \omega_0))} \quad (7)$$

168 Hence, by using the following expression (8), the solar image diameter of a solar parabolic dish
 169 concentrator with a square flat facet can be determined.

$$170 \quad d = D - 2x'' \quad (8)$$

171 2.4 Actual Solar Image location from the vertex (f^*)

172 A shift in the solar image from the focal plane was noticed on the establishment of solar conical angle to
 173 the incident solar radiation and flat facets. Nevertheless, one of the points among the intersection of extreme
 174 reflected rays is on the axis. Hence, for determining the distance of the actual solar image from the vertex, in the
 175 beginning, the point of intersection (f_1 & f_2) of the extreme reflected rays must be determined. Once the points f_1
 176 and f_2 were determined by applying the mathematical theorem, the exact shift can be predicted. The expression
 177 for finding the exact shift of the solar image is given as follows.



178
 179 **Figure 5: Focal region of the parabolic dish with facet considering the conical angle.**

180 Considering the solar image region as shown in Figure 5, the exact shift of the solar image and the solar
 181 image distance from the apex point of the parabola along its axis can be determined by using the following
 182 expression (9).

$$183 \quad f^* = \frac{f_1 + G f_2}{1 + G} \quad (9)$$

184 where, $G = \frac{\tan \rho_1}{\tan \rho_2}$, $\rho_1 = 90 - (2\alpha - \omega_o)$, $\rho_2 = 90 - (2\alpha + \omega_o)$

185 2.5 Determination of Surface Slope Error due to facets (f*)

186 For an ideal parabola, all the incident rays parallel to the axis will converge at the focal point of the
187 parabola. A surface slope error is determined as the angular difference between the actual surface normal and the
188 ideal surface normal of the parabolic surface (Stynes and Ihas 2012). When facets are introduced over the
189 parabolic surface, the alignments of facets impart the surface slope error to the parabolic profile. Applying the
190 following expression, the maximum surface slope error due to facets can be determined (expression 10).

$$191 \quad \theta_r = \frac{\phi}{2} - \alpha \quad (10)$$

192 2.6 Solar Image Calculator

193 Established on the analytical model developed, a portable computer application “Solar Image Calculator”
194 was developed using Python programming language. This lets the users calculate the actual solar image size and
195 the solar image location along the parabolic axis. Rim diameter (D), focal length (f), rim angle (ϕ), length of the
196 facet (L) was taken as the input parameters for the dish concentrator and also the half conical angle (ω_o) was given
197 as solar radiation parameter. Any three parameters out of the dish parameters are required to compute the solar
198 image.

199 2.7 The existing method for determining the solar image

200 The property of parabola is to converge all the rays which are coming parallel to the axis at the focal
201 point. Consequently, hypothetically for an ideal parabola, every single parallel ray concentrates at the focal point.
202 But on account of solar optics, there exists a most conical disc angle of 0.51° because of the bigger sun diameter.
203 On account of this, a little greater solar image will be acquired rather than a point. The formation of the solar
204 image for an ideal parabolic dish concentrator over the focal plane is demonstrated in Figure 6. The reflections at
205 extreme points of the parabolic profile, structure the boundary of the solar image, the outermost reflections are as
206 shown in Figure 6. The existing geometrical optic relations for finding the optimum solar image diameter are
207 expressed by Kaushika which are given below in equations 11 and 12 (Kaushika 1993).

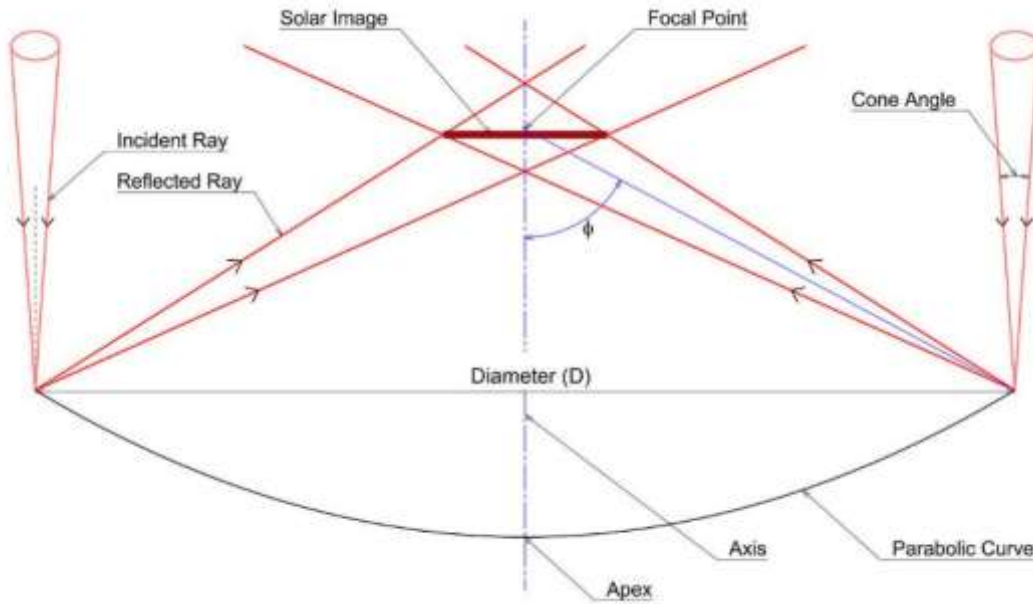
208 The solar image diameter for an ideal paraboloidal dish concentrator:

$$209 \quad d = \frac{4 \times f (\tan \omega_o)}{(1 + \cos \phi)(\cos \phi)} \quad (11)$$

210 for the paraboloidal dish concentrator with facets:

$$211 \quad d = \frac{4 \times f (\tan(\omega_o + \Delta\omega_o))}{(1 + \cos \phi)(\cos \phi)} \quad (12)$$

212 Where, $\Delta\omega_o = \frac{L(1 + \cos \phi) \times 180}{4\pi f}$ is a correction factor based on the facet size, focal length, and rim angle.



213 **Figure 6: Solar Image formation of an ideal parabolic dish concentrator.**

214 **2.7.1 Study of existing analytical model:**

215 To determine the precision and reliability of the existing analytical relationship, it was compared to the
 216 graphical model for various combinations of parabolic dish parameters (dish diameter, rim angle, and facet
 217 length). Three different ranges for parabola geometrical parameters and facet sizes are recorded in Table 1 (from
 218 minimum to maximum values) are used to conduct the numerical experiments.
 219

220 **Table 1: Dataset for parabolic dish parameters and facet sizes**

	Diameter (mm)	Rim Angle (deg.)	Length of facet (mm)
Min	1000	40	40
Max	10000	85	240
Step size	500	5	10

221

222 **2.8 Validation:**

223 The current analytical model has been validated with the available experimental data (Sahu et al. 2020,
 224 2021) in this section. A solar parabolic dish concentrator of 12.5 m² aperture area with square mirror of 0.075 m
 225 side as reflector has been considered for validation of the proposed model. The actual focal image obtained from
 226 the experiment was 0.147 m, whereas the value obtained from the present model is 0.134 m. Therefore, the current
 227 model is in good agreement with deviation of 8.84% with the experimental value. Table 2 shows the specification
 228 of the parabolic concentrator used in the experimental work (Sahu et al. 2020, 2021). Figure 7 shows the parabolic
 229 dish concentrator used for experimental work.

230
231

Table 2: Specifications of dish concentrator (Sahu et al. 2021)

Parameters	Value
Dish Diameter	4 m
Aperture area of dish	12.6 m ²
Rim Angle	45°
F/D ratio	0.6
Facet Shape	Square
Facet Size	0.075 m × 0.075 m
Focal image diameter	0.147 m

232



233
234

Figure 7: Parabolic dish concentrator with square facets(Sahu et al. 2021)

235 3 Result and Discussion

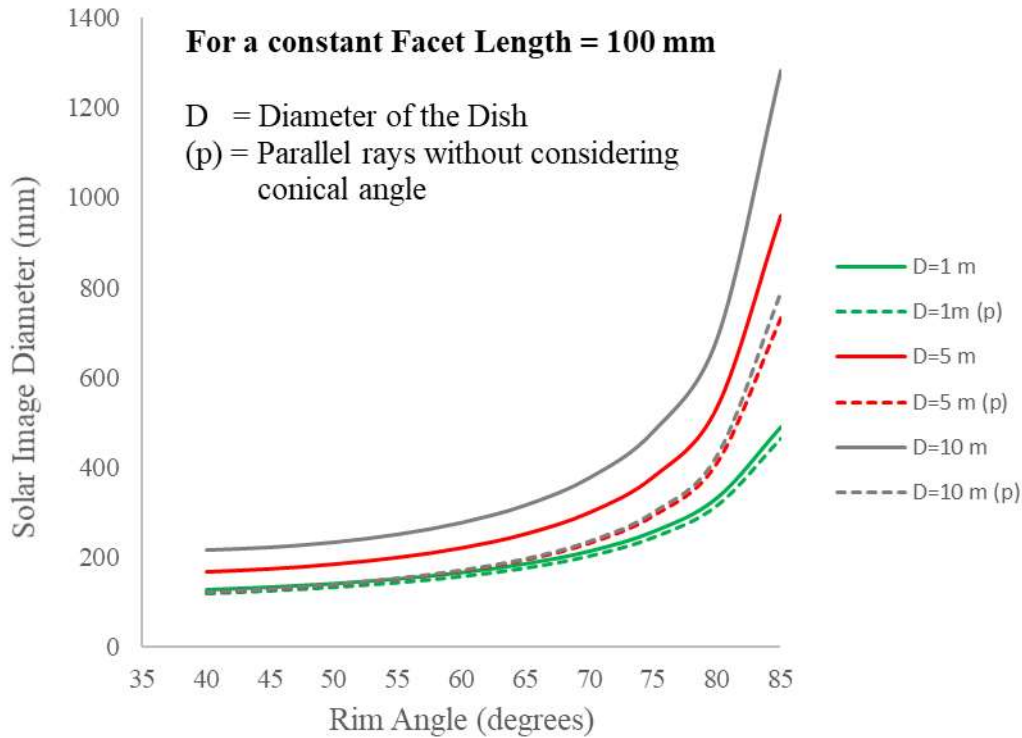
236 Although solar radiations are thought to be parallel beams, their conical angle has a significant impact
237 on the solar image dimension and concentration ratio. The impact of the conical angle, rim angle, facet length,
238 and diameter on parabolic dish characteristics is shown and discussed in this section.

239 3.1 Influence of Conical Angle:

240 In the initial step, solar radiation emanating from the sun is considered as parallel rays (without
241 considering the solar cone angle), where the direction of rays is believed to be parallel to the axis of the parabolic
242 profile. Graphical images have been generated for all the 3990 sets and measured the focal lengths, solar image
243 diameters, and distances of the solar image from the apex automatically employing computer-aided design (CAD)
244 programming.

245 Based on the observations, the influence of conical angle on solar image dimension is depicted in Figure
246 8. By maintaining the facet size constant, the graphical picture depicts the variation of solar image diameter
247 concerning Rim Angle. Only the dish diameters of 1 m, 5 m, and 10 m are used to improve interpretation clarity.
248 As the rim angle increases, the diameter of the solar image expands exponentially. As the diameter of the dish

249 rises, the conical angle has a considerable impact on the solar image diameter. When comparing parallel rays
250 without considering conical angle, it should be noted that the variance in solar image diameter is not as dramatic
251 even with a change in diameter.



252 **Figure 8: Influence of Conical Angle on Solar Image Diameter concerning Rim Angle**
253
254 Because the conical angle affects the solar image, the concentration ratio will be changed as well. Figure
255 9 shows the effect of conical angle on geometrical concentration ratio as a function of rim angle change. The
256 conical angle has a substantial influence on the concentration ratio, as can be seen in the graph. The conical angle
257 influence is less significant for low dish diameters and larger rim angles, according to the results.
258

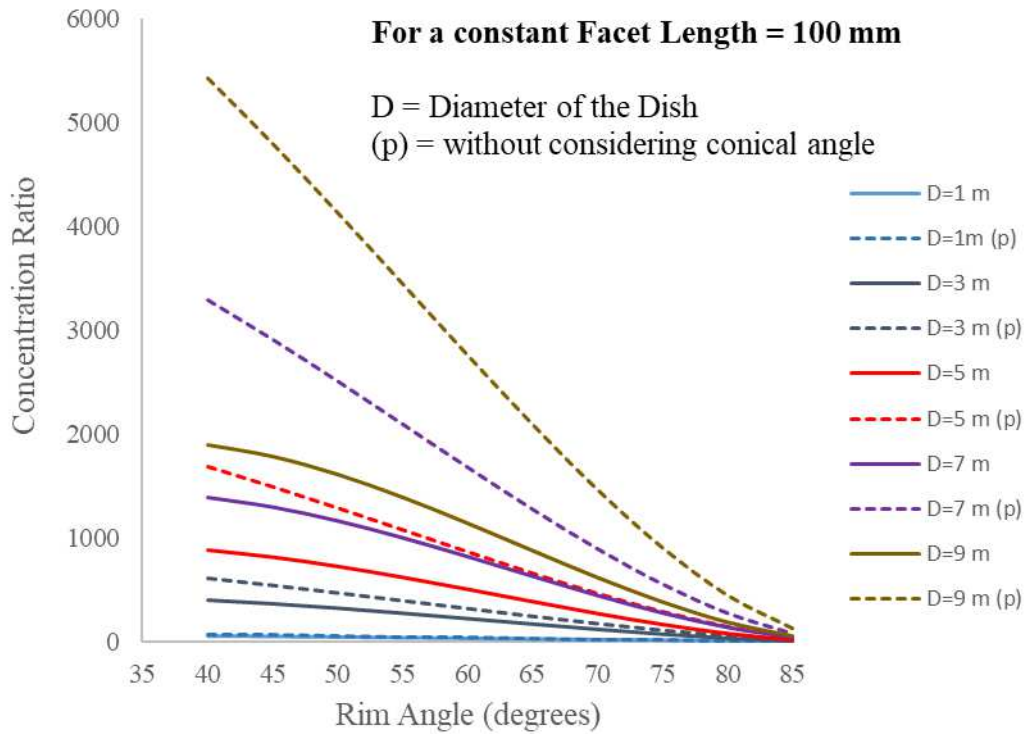


Figure 9: Influence of Conical Angle on Concentration Ratio concerning Rim Angle

259
260

261 **3.2 Prediction of Solar Image Diameter:**

262 The computed and attained solar image diameter are plotted amongst the different design parameters to
263 review the behaviour of the solar image diameter.

264 Figure 10 illustrates the graph between the rim angle (ϕ) and the solar image diameter (d), retaining a
265 constant facet size of 100 mm and dish diameter of six different values (D= 1 m, 2 m, 4 m, 6 m, 8 m, 10 m). It is
266 observed from the illustration that as the rim angle grows the solar image diameter also increases. However, the
267 value of the solar image lies below 500 mm up to 75° rim angle, after that the solar image size increases steeply
268 to the maximum of 1280 mm. Hence, based on this graph it is suggested to choose the parabolic dish concentrator
269 of rim angle less than 75° to get fair performance.

270

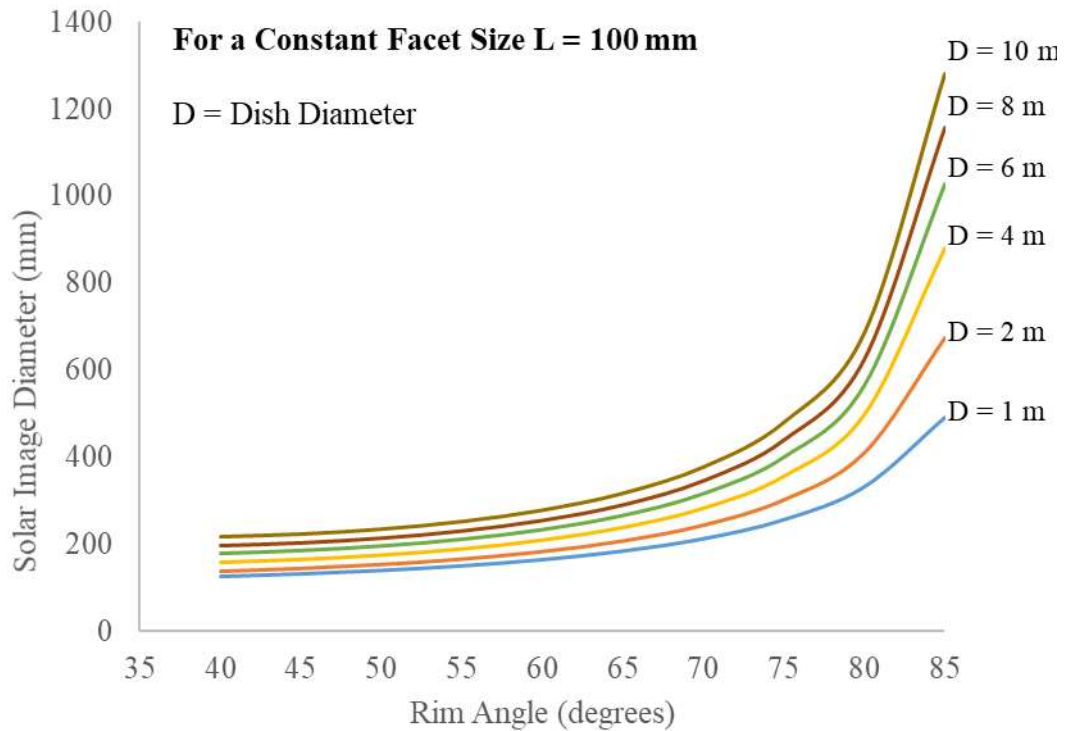


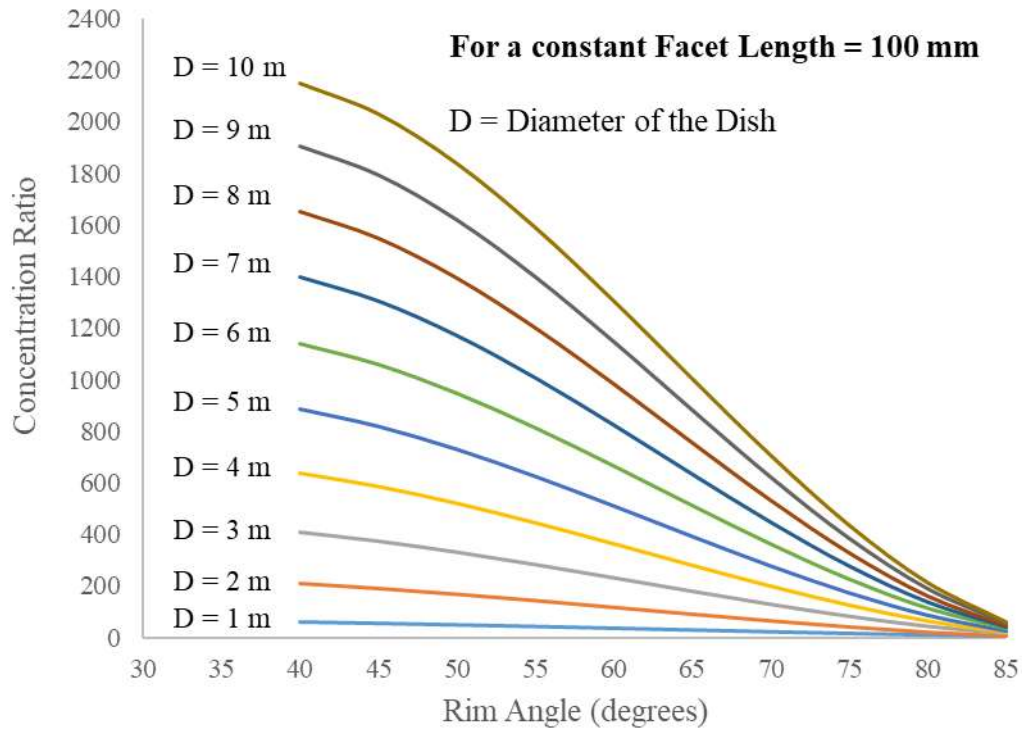
Figure 10: Variation of Solar Image Diameter (d) for Rim angle(ϕ).

271
272

273 The concentration ratio is one of the crucial factors which decides the performance of the solar parabolic
274 dish concentrator system. The geometrical concentration ratio is the ratio of the projected area of the parabolic
275 dish to the area of the receiver. Figure 11 indicates the variation of concentration ratio concerning the rim angle
276 for the developed model for the range of dish diameter considered.

277 On analysing rim angle, the concentration ratio decreases as the rim angle increases. The concentration
278 ratio was noted to be maximum for the lower rim angle in the observed range and showed a significant increase
279 in concentration ratio.

280



281
282

Figure 11: Influence of Rim Angle on Concentration Ratio

283

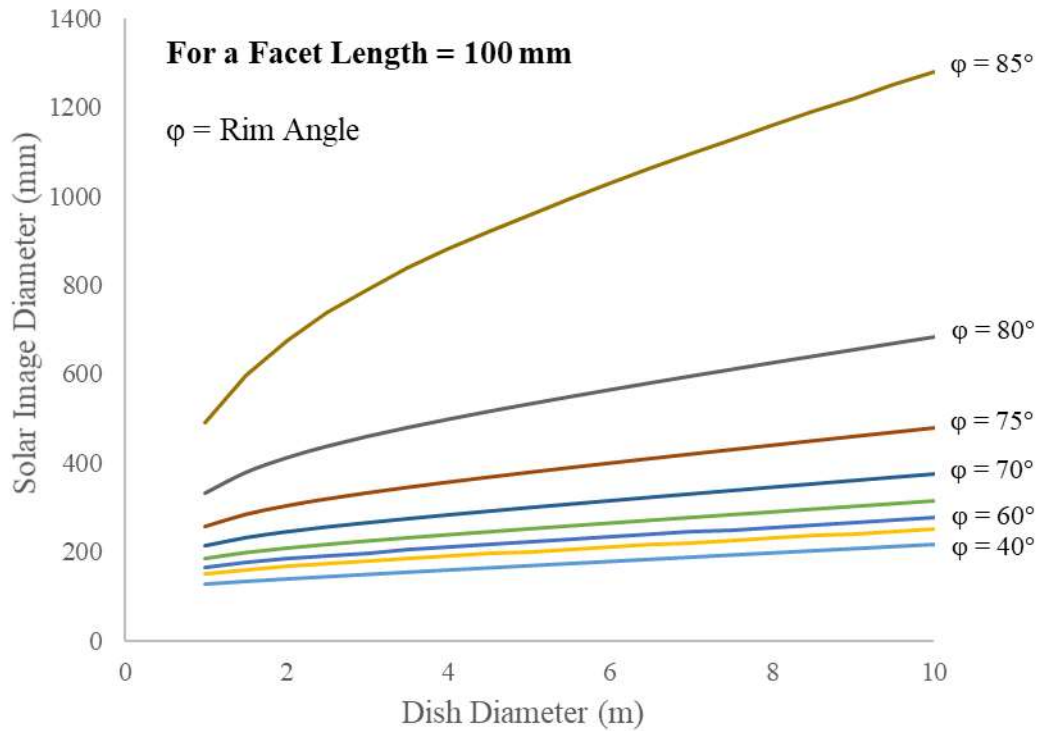
284

285

286

287

Figure 12 illustrates the graph between the dish diameter and the solar image diameter for a constant facet size of 100 mm and rim angle of eight different values ($\phi = 40^\circ, 55^\circ, 60^\circ, 65^\circ, 70^\circ, 80^\circ, 85^\circ$). It reveals that the solar image diameter keeps increasing as the diameter increases irrespective of the facet length and rim angle. However, the trend follows to be linearly increasing up to the rim angle of 75° , above that the variation of solar image diameter is more significant and not linear.



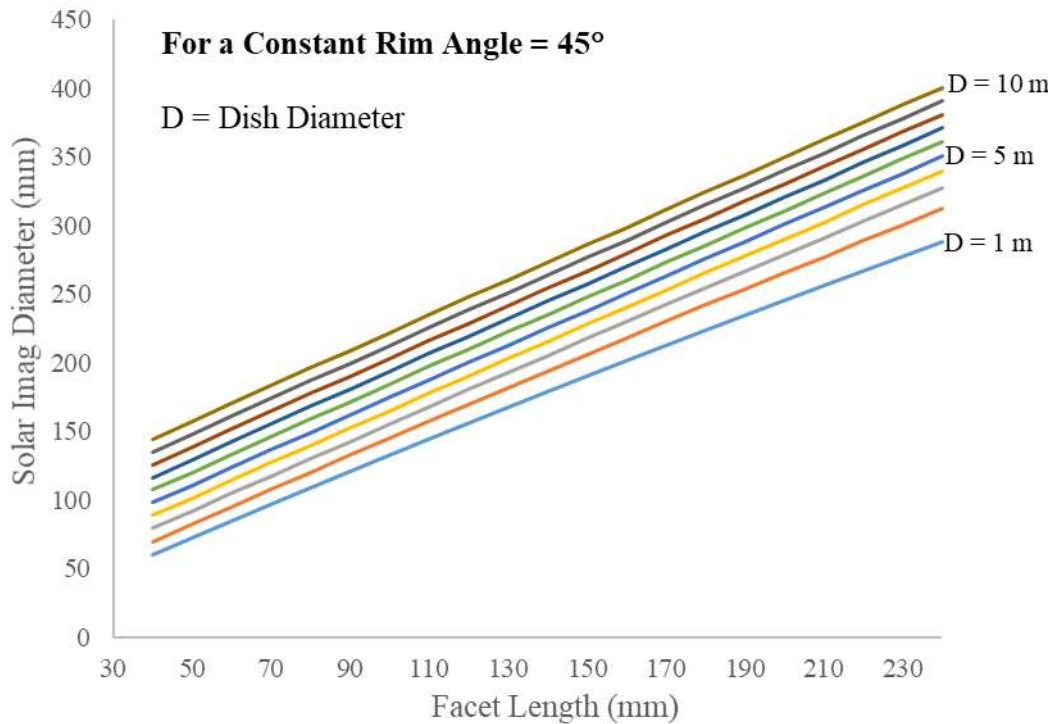
288
289

Figure 12: Variation of Solar Image Diameter (d) for Dish Diameter (D).

290

Figure 13 reveals the variation of solar image diameter in connection with the change in facet size at a constant rim angle of 45° for ten different values of dish diameter (1 m to 10 m). From the graphical illustration, it is found that the solar image size varies linearly as the facet size increases. However, a small deviation from linearity is observed at the lower dish diameters.

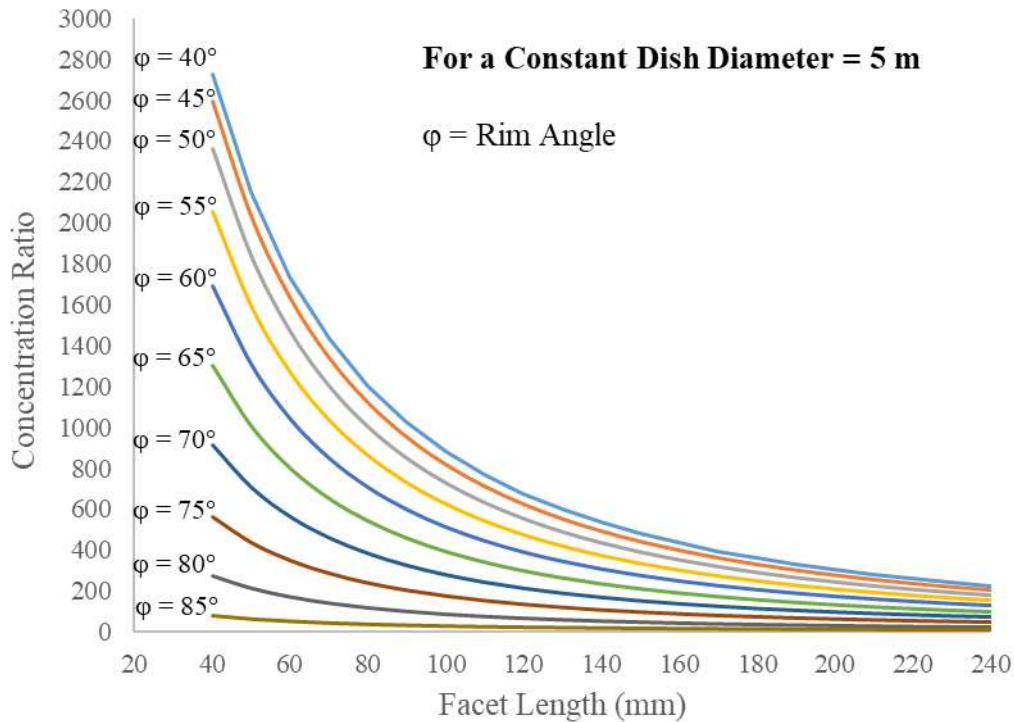
294



295
296

Figure 13: Variation of Solar Image Diameter (d) for the facet size (L).

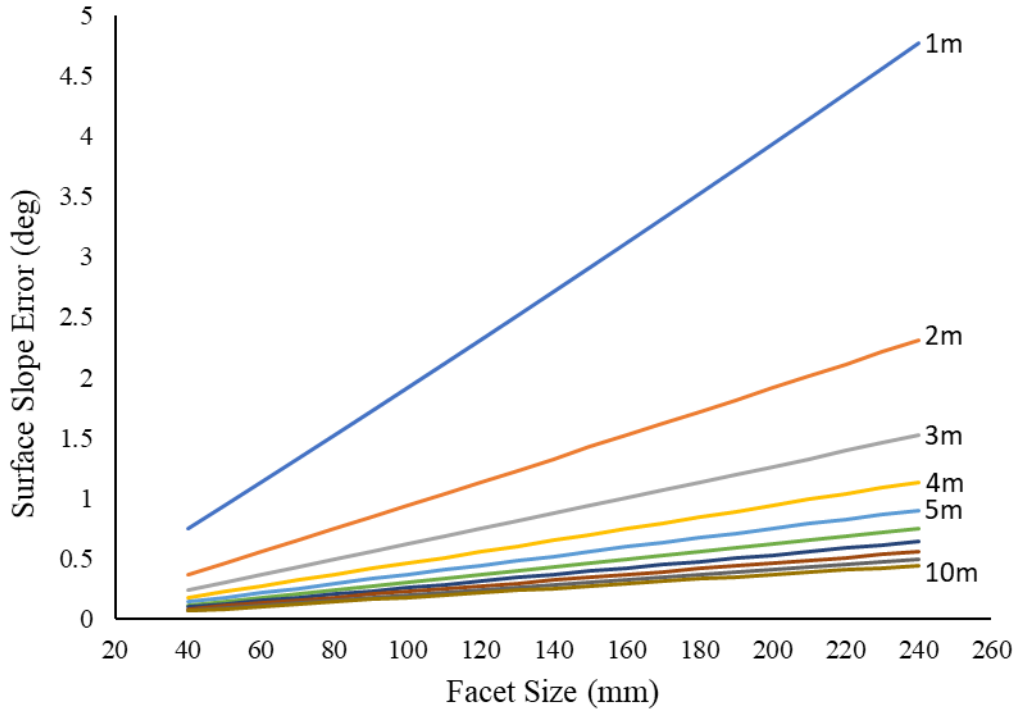
297 Figure 14 illustrates the graph between the concentration ratio and the facet length for a constant dish
 298 diameter of 5 m and rim angle of ten different values from 40° to 85° with an increment of 5°. Based on the graph,
 299 it is observed that the concentration ratio exponentially decreases as the facet size increases. However, the
 300 concentration ratio steeply decreases for greater diameter dishes than the lesser ones. According to the result
 301 analyzed it is suggested to go for fewer size facets for attaining a higher concentration ratio.



302 **Figure 14: Influence of Facet Size on Concentration Ratio**

304 **3.3 Influence of Facet Size on Surface Slope Error:**

305 Figure 15 shows the variation of the surface slope error on a parabolic dish concentrator with a rim angle
 306 of 45° due to the discretized mirror facets over the surface. From the graph, it is observed that the surface slope
 307 error, varies linearly as the facet size is varied. Also, the use of flat facets as an alternative to double curved facet
 308 for concentrator affects the surface with lower slope error for lesser diameter one than the larger diameter dish.
 309 Hence, as per the graph, it can be suggested that the dish diameters of sizes lesser than 5m have minimum surface
 310 slope error compared to higher diameter for the same facet size.



311
312

Figure 15: Influence of Facet Size on Surface Slope Error.

313 **4 Conclusions**

314 Among the point focussing type solar concentrators, the solar parabolic dish got featured because of its
315 superior concentration ratio, better heat flux over the receiver, modular arrangement, and advanced thermal
316 efficiency. The main results of this study can be summarized as below:

- 317 • The proposed technique gives the actual solar image diameter as well as tends to how much
318 drift in the solar image along the axis from the focal plane.
- 319 • Although there is a shift in the actual solar image location the deviation is not so huge. Be that
320 as it may, during the development of larger dishes, the shift ought to be considered for ideal
321 outcomes.
- 322 • By utilizing the proposed model, the specific actual solar image size and area of a solar parabolic
323 dish concentrator with square facets can be resolved.
- 324 • This amplifies the area at which solar radiation incident over the parabolic reflector, as the area
325 blocked by the receiver decreases.
- 326 • The decrease of the solar image distance across prompts a lessening in heat loss from the
327 receiver because of convective and radiative heat transfer, as the receiver surface area shrinks.

- 328
- Likewise, it prompts an expansion in both the geometrical and optical concentration ratio of the parabolic dish concentrator. By acquiring the actual solar image, a high temperature can be gotten on the receiver.
- 329
- 330
- As an extra factor, in view of the reflection point (ρ_1) of the extraordinary radiation, the secondary reflectors or cavity receiver profile can be streamlined.
- 331
- 332
- The characteristic study of surface slope error due to the introduction of flat mirror facet will help the researchers to choose the dish and facet size according to their requirements.
- 333
- 334
- Consequently, the present descriptive model is in good agreement with the experimental value.
- 335
- 336
- As a result, it can be utilized to predict the focal image diameter and its area for the fixed
- 337
- parabolic dish parameters and facet size theoretically.

338 **Declarations**

339 **Ethics approval and consent to participate:** Not applicable

340 **Consent for Publication:** Not applicable

341 **Availability of data and materials:** The datasets used and/or analysed during the current study are available from
342 the corresponding author on reasonable request

343 **Competing interests:** The authors declare that they have no competing interests.

344 **Funding:** Not applicable

345 **Author Contributions - CRediT author statement**

346 **Arjun Singh Kopalakrishnaswami:** Conceptualization, Formal analysis, Investigation, Data Curation, Writing -
347 Original Draft.

348 **Reyhaneh Loni:** Conceptualization, Formal analysis, Investigation, Data Curation, Writing - Original Draft.

349 **Gholamhassan Najafi:** Conceptualization, Validation, Resources, Writing - Review & Editing, Supervision,

350 **Sendhil Kumar Natarajan:** Conceptualization, Validation, Resources, Writing - Review & Editing, Supervision,
351 Project administration.

352 **Acknowledgments**

353 The authors would like to express their gratitude to the National Institute of Technology Puducherry, Karaikal,
354 and Tarbiat Modares University for their support and research facilities.

355

356 **References**

- 357 Farouk Kothdiwala A, Eames PC, Norton B (1996) Optical performance of an asymmetric inverted absorber
358 compound parabolic concentrating solar collector. *Renew Energy* 9:576–579.
359 [https://doi.org/10.1016/0960-1481\(96\)88355-8](https://doi.org/10.1016/0960-1481(96)88355-8)
- 360 Hafez AZ, Soliman A, El-Metwally KA, Ismail IM (2017) Design analysis factors and specifications of solar
361 dish technologies for different systems and applications. *Renew Sustain Energy Rev* 67:1019–1036.
362 <https://doi.org/10.1016/j.rser.2016.09.077>
- 363 Hafez AZ, Soliman A, El-Metwally KA, Ismail IM (2016) Solar parabolic dish Stirling engine system design,
364 simulation, and thermal analysis. *Energy Convers Manag* 126:60–75.
365 <https://doi.org/10.1016/j.enconman.2016.07.067>
- 366 Kalogirou SA (2009) Chapter three - Solar Energy Collectors
- 367 Kaushika ND (1993) Viability aspects of paraboloidal dish solar collector systems. *Renew Energy* 3:787–793.
368 [https://doi.org/10.1016/0960-1481\(93\)90086-V](https://doi.org/10.1016/0960-1481(93)90086-V)
- 369 Kingslake R, Barry Johnson R (2010) Meridional Ray Tracing. *Lens Des Fundam* 25–49.
370 <https://doi.org/10.1016/b978-0-12-374301-5.00006-1>
- 371 Li L, Dubowsky S (2011) A new design approach for solar concentrating parabolic dish based on optimized
372 flexible petals. *Mech Mach Theory* 46:1536–1548. <https://doi.org/10.1016/j.mechmachtheory.2011.04.012>
- 373 Liu Z, Lapp J, Lipiński W (2012) Optical design of a flat-facet solar concentrator. *Sol Energy* 86:1962–1966.
374 <https://doi.org/10.1016/j.solener.2012.03.007>
- 375 Østergaard PA, Duic N, Noorollahi Y, et al (2020) Sustainable development using renewable energy
376 technology. *Renew Energy* 146:2430–2437. <https://doi.org/10.1016/j.renene.2019.08.094>
- 377 Pavlovic´ SR, Stefanovic´ VP, Suljkovic´ SH (2014) Optical modeling of a solar dish thermal concentrator
378 based on square flat facets. *Therm Sci* 18:989–998. <https://doi.org/10.2298/TSCI1403989P>
- 379 Pavlovic SR, Stefanovic VP (2015) Ray Tracing Study of Optical Characteristics of the Solar Image in the
380 Receiver for a Thermal Solar Parabolic Dish Collector. *J Sol Energy* 2015:1–10.
381 <https://doi.org/10.1155/2015/326536>
- 382 Pavlović SR, Vasiljević DM, Stefanović VP, et al (2016) Optical analysis and performance evaluation of a solar
383 parabolic dish concentrator. *Therm Sci* 20:S1237–S1249. <https://doi.org/10.2298/TSCI16S5237P>
- 384 S P Sukhatme, Nayak JK (2017) *Solar Energy, Fourth*. McGraw Hill
- 385 Sahu SK, Arjun Singh K, Natarajan SK (2020) Design and development of a low-cost solar parabolic dish
386 concentrator system with manual dual-axis tracking. *Int J Energy Res* 1–11.
387 <https://doi.org/10.1002/er.6164>
- 388 Sahu SK, K AS, Natarajan SK (2021) Impact of double trumpet-shaped secondary reflector on flat receiver of a
389 solar parabolic dish collector system. *Energy Sources, Part A Recover Util Environ Eff* 00:1–19.
390 <https://doi.org/10.1080/15567036.2021.1918803>
- 391 Singh NP, Reddy KS (2020) Inverse heat transfer technique for estimation of focal flux distribution for a
392 concentrating photovoltaic (CPV) square solar parabola dish collector. *Renew Energy* 145:2783–2795.
393 <https://doi.org/10.1016/j.renene.2019.07.122>
- 394 Stynes JK, Ihas B (2012) Slope Error Measurement Tool for Solar Parabolic Trough Collectors
- 395 Toygar EM, Bayram T, Daş O, Demir A (2016) The design and development of solar flat mirror (Solarux)
396 system. *Renew Sustain Energy Rev* 54:1278–1284. <https://doi.org/10.1016/j.rser.2015.10.085>
- 397 Waghmare SA, Gulhane NP (2019) Design configurations and possibilities of reflector shape for solar
398 compound parabolic collector by ray tracing simulation. *Optik (Stuttg)* 176:315–323.
399 <https://doi.org/10.1016/j.ijleo.2018.09.082>
- 400 Wen L, Huang L, Poon P, Carley W (1980) Comparative study of solar optics for paraboloidal concentrators. *J*
401 *Sol Energy Eng Trans ASME* 102:305–315. <https://doi.org/10.1115/1.3266196>
- 402 Xiao L, Guo FW, Wu SY, Chen ZL (2020) A comprehensive simulation on optical and thermal performance of
403 a cylindrical cavity receiver in a parabolic dish collector system. *Renew Energy* 145:878–892.
404 <https://doi.org/10.1016/j.renene.2019.06.068>

405 Yan J, Peng Y duo, Cheng Z ran (2018) Optimization of a discrete dish concentrator for uniform flux
406 distribution on the cavity receiver of solar concentrator system. *Renew Energy* 129:431–445.
407 <https://doi.org/10.1016/j.renene.2018.06.025>
408

Supplementary Files

This is a list of supplementary files associated with this preprint. Click to download.

- [supplementaryDoc.pdf](#)